ARTICLES
https://doi.org/10.1038/s41587-019-0205-0
nature biotechnology

A divalent siRNA chemical scaffold for potent and sustained modulation of gene expression throughout the central nervous system

Julia F. Alterman[1,13], Bruno M. D. C. Godinho[1,13], Matthew R. Hassler[1,13], Chantal M. Ferguson[1,13], Dimas Echeverria[1], Ellen Sapp[2], Reka A. Haraszti[1], Andrew H. Coles[1], Faith Conroy[1,3], Rachael Miller[1,3], Loic Roux[1], Paul Yan[1], Emily G. Knox[1], Anton A. Turanov[1], Robert M. King[4,5], Gwladys Gernoux[6], Christian Mueller[6,7], Heather L. Gray-Edwards[4], Richard P. Moser[8], Nina C. Bishop[9], Samer M. Jaber[9,10], Matthew J. Gounis[4], Miguel Sena-Esteves[6,11], Athma A. Pai[1], Marian DiFiglia[2], Neil Aronin[1,3] and Anastasia Khvorova[1,12]*

Sustained silencing of gene expression throughout the brain using small interfering RNAs (siRNAs) has not been achieved. Here we describe an siRNA architecture, divalent siRNA (di-siRNA), that supports potent, sustained gene silencing in the central nervous system (CNS) of mice and nonhuman primates following a single injection into the cerebrospinal fluid. Di-siRNAs are composed of two fully chemically modified, phosphorothioate-containing siRNAs connected by a linker. In mice, di-siRNAs induced the potent silencing of huntingtin, the causative gene in Huntington's disease, reducing messenger RNA and protein throughout the brain. Silencing persisted for at least 6 months, with the degree of gene silencing correlating to levels of guide strand tissue accumulation. In cynomolgus macaques, a bolus injection of di-siRNA showed substantial distribution and robust silencing throughout the brain and spinal cord without detectable toxicity and with minimal off-target effects. This siRNA design may enable RNA interference-based gene silencing in the CNS for the treatment of neurological disorders.

Oligonucleotide therapeutics are an emerging class of drugs that enable potent and efficient modulation of gene expression in vivo[1]. An outstanding challenge is developing chemical architectures of oligonucleotides that permit robust, productive and safe delivery to a particular target tissue. The delivery and functionality of siRNAs and antisense oligonucleotides (ASOs) have been established for the liver[2,3] and recent efforts have shifted towards delivery to other organs, including the CNS[4,5].

The siRNAs are large, negatively charged, double-stranded molecules that require formulation[6] or chemical conjugation[7–10] for delivery to tissues. When fully chemically stabilized siRNAs are conjugated to hydrophobic ligands such as cholesterol[7], docosahexaenoic acid (DHA)[8] or DHA with a phosphocholine head group[10], they are successfully internalized by brain cells[11]; however, they are retained near the brain injection site, even with continuous monthly administration[4,7]. Thus, other modification strategies are needed to expand siRNA distribution and efficacy in the CNS.

Broad distribution of ASOs, systemically and in the CNS, has been achieved primarily using phosphorothioate (PS) backbone modifications[12]. The most advanced CNS-active ASO scaffold utilizes a mixed backbone configuration with at least 70–80% PS content. This modification maintains efficacy and distribution with minimal risk of toxic phenotypes[13,14] via mechanisms that are not fully understood[15]. PS modifications are also essential for clinically advanced siRNA configurations[1,16]; however, increasing the PS content of individual siRNA duplexes to 80% can limit RNA-induced silencing complex (RISC) efficacy[17,18] and increase toxicity[19,20].

An alternative approach may be multivalency, that is, cooperative interactions between multiple partially PS-modified siRNAs. Indeed, the most clinically advanced siRNA conjugate is the multivalent *N*-acetylgalactosamine (GalNAc)[21] that drives delivery to and silencing in the liver. A single subcutaneous injection of trivalent GalNAc-conjugated siRNA can achieve efficacy for >12 months[22–24].

Here we describe a divalent chemical scaffold of fully chemically modified, PS-containing siRNAs (di-siRNAs) that provide widespread distribution and sustained gene silencing in the rodent and nonhuman primate (NHP) brain after a single administration into the cerebrospinal fluid (CSF). To characterize the novel scaffold, we used an siRNA sequence targeting huntingtin (*HTT*), the causative gene in Huntington's disease (HD)[4].

[1]RNA Therapeutics Institute, University of Massachusetts Medical School, Worcester, MA, USA. [2]Department of Neurology, Massachusetts General Institute for Neurodegenerative Disease, Boston, MA, USA. [3]Department of Medicine, University of Massachusetts Medical School, Worcester, MA, USA. [4]Department of Radiology, New England Center for Stroke Research, University of Massachusetts Medical School, Worcester, MA, USA. [5]Department of Biomedical Engineering, Worcester Polytechnic Institute, Worcester, MA, USA. [6]Horae Gene Therapy Center, University of Massachusetts Medical School, Worcester, MA, USA. [7]Department of Pediatrics, University of Massachusetts Medical School, Worcester, MA, USA. [8]Department of Neurosurgery, University of Massachusetts Medical School, Worcester, MA, USA. [9]Department of Animal Medicine, University of Massachusetts Medical School, Worcester, MA, USA. [10]Department of Pathology, University of Massachusetts Medical School, Worcester, MA, USA. [11]Department of Neurology, University of Massachusetts Medical School, Worcester, MA, USA. [12]Program in Molecular Medicine, University of Massachusetts Medical School, Worcester, MA, USA. [13]These authors contributed equally: Julia F. Alterman, Bruno M.D.C. Godinho, Matthew R. Hassler, Chantal M. Ferguson.
*e-mail: anastasia.khvorova@umassmed.edu

Results

Structure and synthesis of di-siRNAs. As full chemical modification of siRNAs is essential for conjugate-mediated delivery[16], we used fully chemically modified asymmetric siRNAs that have a 20-base guide strand and 15-base passenger strand. All terminal backbone positions and the protruding 3′ end of the guide strand are fully phosphorothioated, resulting in PS modifications to 13 out of 35 phosphate linkages (~40% PS content) (Fig. 1a). These unconjugated siRNAs exhibit minimal brain retention and distribution (Fig. 1b).

Di-siRNA was synthesized using a functionalized solid support (Supplementary Fig. 1), which allowed for parallel growth of two oligonucleotides. As a result, two sense strands are covalently connected at their 3′ end through a tetraethylene glycol linker. Use of the polymeric spacer was necessary to limit steric hindrance during synthesis and functional knockdown. Annealing of the passenger strand to two identical 20-base guide strands formed a ~27 kD compound (Fig. 1c). Mono- and di-siRNAs show comparable in vitro half-maximum inhibitory concentration (IC_{50}) values (Supplementary Fig. 2), suggesting that linking the two molecules does not compromise RISC loading. The sequences and chemical configuration of all compounds used in this study are shown in Supplementary Table 1.

Di-siRNA shows widespread retention after an intraparenchymal injection. Intraparenchymal injection of Cy3-labeled di-siRNA enhanced the distribution and retention in the mouse brain compared to Cy3-labeled monovalent siRNA (Fig. 1d), supporting the idea that a cooperative interaction between two partially PS-modified siRNAs is sufficient for widespread brain retention. In all experiments, the dose of injected compounds (mono versus di-siRNA) was defined by guide strand concentration (that is, di-siRNA injection includes half the number of molecules compared to the mono-siRNA injection).

di-siRNA targeting *Htt* mRNA was synthesized using a previously identified siRNA sequence[7]. Intrastriatal injection of di-siRNA^{HTT} in wild-type mice resulted in potent downregulation of *Htt* mRNA (between 50% and 75%) in the striatum and cortex 2 weeks after injection (Supplementary Fig. 3a). Both Cy3-labeled and non-labeled di-siRNA^{HTT} show similar levels of silencing in the cortex and striatum (~80% silencing, $P<0.0001$, Supplementary Fig. 3b), whereas the nontargeting control (NTC) oligonucleotide did not impact target gene expression (Supplementary Fig. 3a,b).

We also synthesized di-siRNA^{HTT} variants containing fewer and no PS backbone modifications (Supplementary Fig. 4a). Reducing the number of PS modifications reduced silencing efficacy, and completely removing PS modifications fully abolished activity (Supplementary Fig. 4b), after intrastriatal injection in mice. Thus, the observed efficacy of di-siRNA^{HTT} is mediated by PS modification.

Distribution and silencing by di-siRNA after CSF injection. To evaluate the CSF-driven brain distribution of Cy3-di-siRNA, we injected 475 µg intracerebroventricularly (ICV) into the lateral ventricles of mice. After 48 h from the injection, the mouse brain was uniformly pink to the naked eye (Fig. 1e), indicating a broad distribution. Microscopy confirmed our initial observation (Fig. 1f). Di-siRNAs had distributed to all regions of the brain, from the prefrontal cortex to the cerebellum. High-magnification images show an accumulation in the vast majority of neurons (Fig. 1g,h). Intracellular distribution followed a perinuclear localization pattern that is characteristic of oligonucleotides[11].

Broad distribution of di-siRNA^{HTT} supported productive silencing 2 weeks after injection in all brain regions, including prefrontal, medial and posterior cortices, striatum, hippocampus, thalamus, hypothalamus, cerebellum, brain stem and cervical, thoracic and lumbar sections of the spinal cord (Supplementary Fig. 5). To quantitatively evaluate guide strand accumulation, we used a peptide nucleic acid hybridization assay, which provides quantitative accumulation data and does not depend on the presence of a fluorescent label[25]. Analysis (Supplementary Fig. 5a) confirmed the visual and microscopy-based observations of broad di-siRNA distribution, and correlated with *Htt* mRNA (Supplementary Fig. 5b) and HTT protein (Supplementary Fig. 5c,d) silencing.

Next, we compared the efficacy of two different di-siRNA^{HTT} doses, 60 µg and 475 µg, 1 month after injection in wild-type mice (Supplementary Fig. 6a). The higher dose resulted in approximately a twofold maximum increase in guide strand tissue retention and a wider distribution compared to the lower dose (0.1 to 4 µg g^{-1} at 60 µg; 2–8 µg g^{-1} at 475 µg, Supplementary Fig. 6b). The higher dose silenced the HTT protein below the level of detection ($P<0.0001$) throughout the brain (Fig. 1i and Supplementary Fig. 7). The lower dose was efficacious in the hippocampus, thalamus and striatum, showing 80–99% silencing ($P<0.0001$, $P<0.001$ and $P<0.0001$, respectively). Efficacy was reduced in the cortical areas located away from the site of injection, consistent with the relatively lower guide strand accumulation in these regions. The NTC and PBS groups showed no difference in HTT expression levels. NTC was used as a control for all subsequent experiments (Fig. 1i).

Di-siRNAs silence other genes in the CNS. The chemical architecture of an siRNA determines pharmacokinetics and tissue delivery but the base sequence of the oligonucleotide determines its target. To evaluate the programmability of the di-siRNA scaffold, we measured its efficacy when targeted to other mRNAs in the CNS.

Following intrastriatal injection of di-siRNA targeting cyclophilin B (*Ppib*), we observed potent *Ppib* silencing (65–85%, $P<0.0001$; Supplementary Fig. 8). The NTC control had no activity, demonstrating that silencing was specific to the *Ppib*-targeting sequence. Recently, we identified functional siRNA sequences targeting apolipoprotein E (ApoE), implicated in several neurodegenerative diseases, including Alzheimer's disease and amyotrophic lateral sclerosis[26–28] (Ferguson et al., manuscript in preparation). We synthesized di-siRNA^{APOE} (see Supplementary Table 1 for sequence information) and injected mice ICV with PBS and NTC as controls. A single CSF injection of di-siRNA^{APOE} resulted in potent silencing (>95%) of APOE protein after one month (Fig. 1j and Supplementary Fig. 10). NTC had no impact on APOE expression, indicating that the observed silencing is sequence specific. The observed protein silencing correlated well with mRNA silencing (Supplementary Fig. 10). Thus, the di-siRNA chemical scaffold can be reprogrammed to modulate gene expression in vivo for multiple targets implicated in the pathogenesis of neurological conditions.

High-dose di-siRNA silencing for at least 6 months. To evaluate the duration of di-siRNA efficacy, we delivered a high dose (475 µg) of di-sRNA^{HTT} or di-siRNA^{NTC} to wild-type mice via a single ICV injection. We measured guide strand accumulation levels, *Htt* mRNA, and HTT protein in key brain regions (cortex, striatum, thalamus, hippocampus) at 1, 4 and 6 months after injection (Fig. 2a). Guide strand accumulation in different brain regions ranged between 2 and 7 µg g^{-1} at 1 month, 0.8 and 2.5 µg g^{-1} at 4 months and 0.2 and 1.8 µg g^{-1} at 6 months, suggesting relatively slow clearance (Fig. 2b).

The extent of HTT protein silencing was always greater than *Htt* mRNA (>99% versus ~70%) (Fig. 2c,d) because a fraction of *Htt* mRNA localizes to the nucleus, making it more resistant to RNA interference-based silencing[29]. More than 80% silencing of HTT protein was maintained at 4 months in all brain regions analyzed (Fig. 2d and Supplementary Figs. 7 and 11 for raw westerns). At 6 months, the degree of silencing differed between brain regions: >90% in the hippocampus, ~50% in the thalamus and striatum and high variability in the cortex.

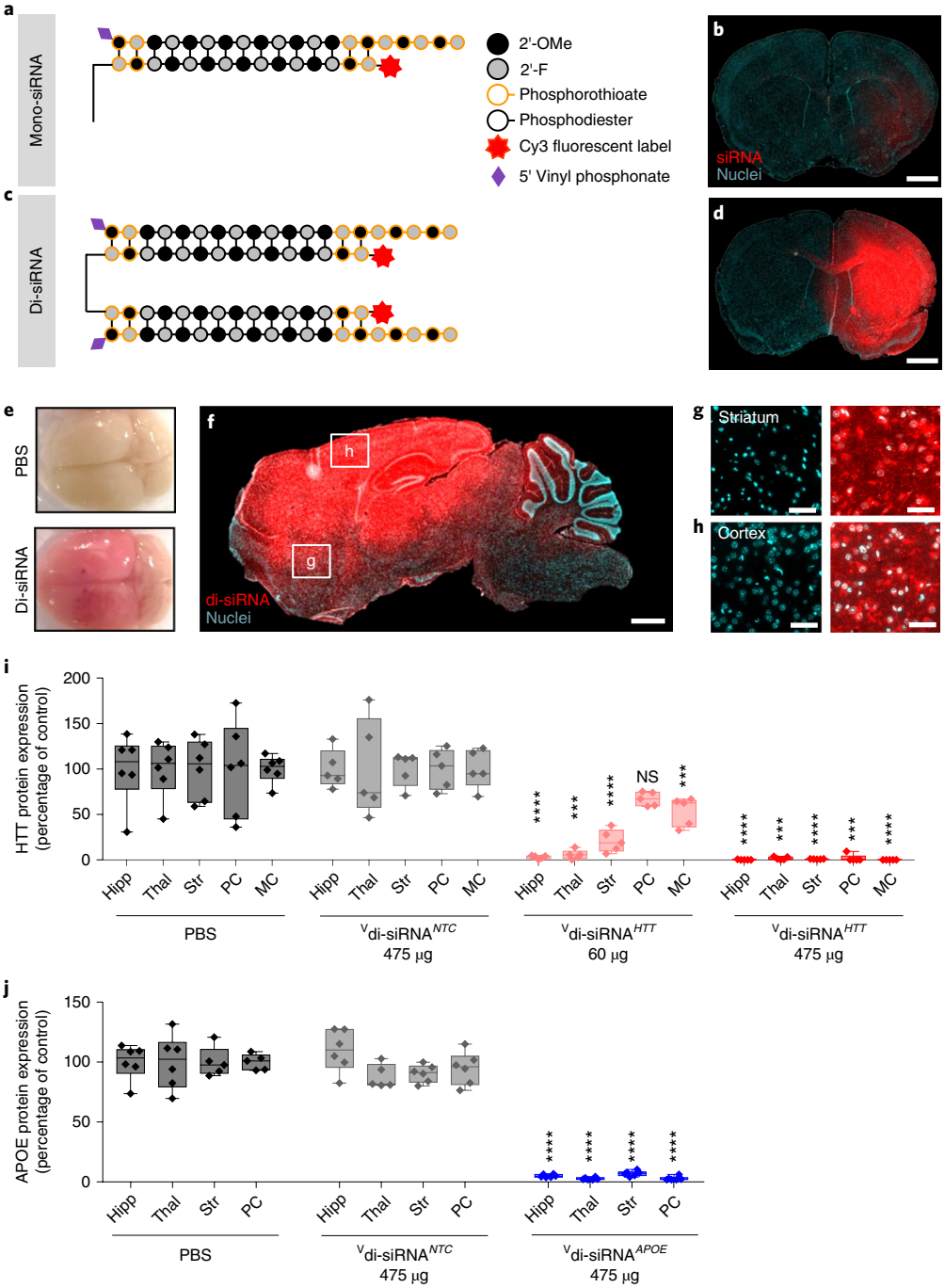

Fig. 1 | A divalent siRNA chemical configuration enables gene silencing in the mouse brain. a, Schematic of the chemical structure of mono-siRNA. **b**, Biodistribution of Cy3-labeled mono-siRNA 48 h after a single intrastriatal injection of 50 µg. Scale bar, 1 mm. **c**, Schematic of the chemical structure of di-siRNA. **d**, Biodistribution of Cy3-labeled di-siRNA 48 h after a single intrastriatal injection of 50 µg. Scale bar, 1 mm. **e**, Image of whole mouse brain injected with di-siRNA (top, PBS; bottom, di-siRNA) Scale bar, 2.5 mm. **f**, di-siRNA distributes throughout the mouse brain after a bilateral injection of 475 µg (237 µg per ventricle) into the lateral ventricles. Tiled fluorescent images taken 48 h after injection. Scale bar, 1 mm. **g,h**, High-resolution images of di-siRNA distribution to various regions of the mouse brain: striatum (**g**) and cortex (**h**). Scale bar, 50 µm. **i**, di-siRNA silences the HTT protein at two different doses in multiple brain regions 1 month after bilateral ICV injection. All statistics are one-way analysis of variance (ANOVA) with Dunnett's multiple comparisons test. All results are compared to PBS control. Hipp: $F(3,17) = 31.92$, HTT 60 µg $^{****}P < 0.0001$, HTT 475 µg $^{****}P < 0.0001$. Thal: $F(3,17) = 16.875$, HTT 60 µg $^{***}P = 0.0003$, HTT 475 µg $^{***}P = 0.0002$. Str: $F(3,17) = 33.38$, HTT 60 µg $^{****}P < 0.0001$, HTT 475 µg $^{****}P < 0.0001$. PC: $F(3,17) = 12.64$, HTT 475 µg $^{***}P = 0.0001$. MC: $F(3,17) = 53.58$, HTT 60 µg $^{***}P = 0.0003$, HTT 475 µg $^{****}P < 0.0001$. PBS: $n = 6$, NTC $n = 5$, HTT 60 µg: $n = 5$, HTT 475 µg: $n = 5$. Mean ± s.d. Hipp, hippocampus; Thal, thalamus; Str, striatum; PC, posterior cortex; MC, medial cortex. **j**, di-siRNA silences apolipoprotein E (APOE) protein 1 month after bilateral ICV injection. All statistics are one-way ANOVA with Dunnett's multiple comparisons test. All results are compared to PBS control. Hipp: $F(2,14) = 1.991$, $^{****}P < 0.0001$. Thal: $F(2,14) = 4.283$, $^{****}P < 0.0001$. Str: $F(2,15) = 4.781$, $^{****}P < 0.0001$. PC: $F(2,14) = 6.618$, $^{****}P < 0.0001$. PBS: $n = 6$. NTC mean ± s.d. NS, not significant.

Di-siRNA retention correlates with mRNA and protein silencing. Using data from all time points in the duration of effect study, we observed strong correlations between the level of residual guide strand accumulation and the degree of *Htt* mRNA (Fig. 2e) and HTT protein (Fig. 2f) silencing. We estimate the protein silencing IC_{50} value to be ~0.5 μg g^{-1} and the IC_{90} value to be ~2 μg g^{-1} of guide strand accumulation in tissues.

Figure 2g shows guide strand clearance over time for individual brain regions. Initial (1 month) hippocampal accumulation of ~7 μg g^{-1} resulted in ~2 μg g^{-1} present at 6 months. Both levels of guide strand accumulation are sufficient to silence HTT protein below the level of detection. In the cortical regions, the initial accumulation at 1 month was 3–4 μg g^{-1} and fell below the 0.5 μg g^{-1} threshold by 6 months resulting in a loss of silencing in some animals. This suggests that siRNA tissue accumulation at early time points can be used to estimate the duration of effect.

Di-siRNA is safe and well tolerated in mice. Next, we evaluated the safety and tolerability of di-siRNA at 475 μg over 6 months. To assess neuronal viability, we measured DARPP32 protein expression, an established marker for medium spiny neurons in the striatum[7]. Loss of DARPP32 indicates neuronal death. Injection of di-siRNA had no impact on DARPP32 expression (Supplementary Figs. 7 and 11). To evaluate the impact of di-siRNA injection on microglia activation and gliosis, we measured two well-established markers of immune stimulation, IBA-1 and glial fibrillary acidic protein (GFAP). IBA-1 is located within a major histocompatibility complex and increases as a result of microglial activation[7]. GFAP is an intermediate filament protein and increases as a result of astrocyte proliferation[30]. We observed only minor changes in *Iba-1* expression (<1.5-fold from control) at both doses and at all three time points. At the higher dose, we observed transient *Gfap* activation at 1 month, but this disappeared by 4 months (Supplementary Figs. 12 and 13). Finally, a comprehensive blood chemistry panel showed no detectable changes at any time point, suggesting a systemic tolerability of di-siRNA administration to the CNS (Supplementary Fig. 14). Overall, di-siRNA injection in CSF was well tolerated in mice at the doses and time points tested.

Di-siRNA silences both wild-type and mutant HTT protein. Di-siRNA^{HTT} is perfectly complementary to both human *HTT* and mouse *Htt* genes[7]. To evaluate the ability of di-siRNA^{HTT} to silence mutant *HTT*, we measured the efficacy in the BACHD-ΔN17 mouse model of HD. This HD model contains wild-type mouse *Htt* and mutant human *HTT* (97 CAG repeats) with 17 N-terminal amino acids removed[31]. At 7 weeks old, animals were injected with 475 μg of di-siRNA targeting *HTT* or NTC or with PBS. HTT protein expression was evaluated at 5 months of age (~3 months after injection). We used a combination of two antibodies (Ab1 and 1C2) to evaluate specific knockdown of wild-type mouse and mutant human HTT protein. The Ab1 antibody only detects wild-type HTT protein as its epitope is located in exon 1 (ref. [32]). The 1C2 antibody detects polyQ expansions[33] and thus, is specific to the mutant protein. A single injection of di-siRNA^{HTT} showed potent downregulation of both mutant and wild-type HTT protein (Supplementary Fig. 15), with a silencing efficiency similar to that in wild-type mice at 4 months after injection (Fig. 2d). This finding suggests that di-siRNA can be used to silence both mutant and wild-type *HTT* expression.

Di-siRNA distributes and silences in the NHP brain. Rodent systemic distribution is generally predictive of large mammal distribution, although this is not necessarily the case for the CNS. Complexity of brain structure, CSF volume, rate of clearance and the overall distance of brain regions from the CSF may contribute to oligonucleotide distribution and retention. We evaluated the distribution, efficacy and safety of a single CSF injection of di-siRNA in the cynomolgus macaque, whose siRNA-targeting region in the *HTT* sequence is equivalent to that in mice and humans.

We delivered di-siRNA^{HTT} via ICV injection, using magnetic resonance imaging (MRI) and computerized tomography (CT) to confirm needle placement in the lateral ventricle. A 25-mg dose in 750 μl of PBS was infused over 10 min (see Methods). Animals woke up within 15 min after anesthesia was discontinued, with no observable adverse events (Fig. 3a). After 48 h from the unilateral injection, we observed uniform distribution throughout the NHP brain, similar to mice. The injected oligonucleotide was fluorescently labeled, allowing for visual and microscopy-based distribution evaluation. The brain appeared visibly pink with no obvious difference in the degree of oligonucleotide distribution in injected versus noninjected sides (Fig. 3b). Upon sectioning of the brain, we observed uniform cortical distribution with evident delivery to deep brain structures, including the striatum (caudate and putamen) and hippocampus (Fig. 3c). Fluorescent microscopy confirmed the visual distribution, with delivery to the cortex, caudate and hippocampus.

To evaluate any potential preference for specific cell types, we performed immunofluorescence on sections of di-siRNA-treated NHP brains using neuron-specific (NeuN)[34] and glial cell-specific (GFAP)[35] antibodies. We observed an efficient distribution of di-siRNA to both neurons and glial cells in the hippocampus and cortex, and observed colocalization of di-siRNA (red) with both neurons (green) and glial cells (purple) (Fig. 3d). This finding suggests that di-siRNA could be used to treat neurological conditions affecting multiple cell types.

At 1 month after injection (Fig. 3e), we observed 1–9 μg g^{-1} guide strand accumulation, with the highest accumulation detected in the cortex (9 μg g^{-1}), hippocampus (6 μg g^{-1}) and thalamus (6 μg g^{-1}), and the lowest accumulation in the caudate (2 μg g^{-1}) and

Fig. 2 | Di-siRNA efficacy is sustained in mice 6 months after a single bilateral ICV injection. Mice were injected with 475 μg siRNA (bilaterally) (237 μg per ventricle) and data was collected at 1, 4, and 6 months after injection. **a**, Schematic of the duration of effect study in mice. **b**, Guide strand accumulation (μg g^{-1}) in five brain regions. Hipp, hippocampus; Thal, thalamus; Str, striatum; PC, posterior cortex; MC, medial cortex. **c**, *Htt* mRNA silencing (percentage of control) in five brain regions. All statistics are two-tailed unpaired *t*-tests. All results are compared to NTC control. 1 month. Hipp: $t = 9.56$, d.f. = 8, ****$P < 0.0001$. Thal: $t = 10.59$, d.f. = 8, ****$P < 0.0001$. Str: $t = 10.63$, d.f. = 8, ****$P < 0.0001$. PC: $t = 11.45$, d.f. = 8, ****$P < 0.0001$. MC: $t = 8.082$, d.f. = 8, ****$P < 0.0001$. HTT: $n = 5$, NTC: $n = 5$. 4 months. Hipp: $t = 14.26$, d.f. = 9, ****$P < 0.0001$. Thal: $t = 8.577$, d.f. = 9, ****$P < 0.0001$. Str: $t = 6.606$, d.f. = 9, ****$P < 0.0001$. PC: $t = 2.561$, d.f. = 9, *$P = 0.0306$. HTT: $n = 6$, NTC: $n = 5$. 6 months. Hipp: $t = 6.998$, d.f. = 7, ***$P = 0.0002$. Thal: $t = 9.865$, d.f. = 7, ****$P < 0.0001$. Str: $t = 4.264$, d.f. = 7, **$P = 0.0037$. HTT: n = 5, NTC: $n = 4$. **d**, HTT protein silencing (% of control) in five brain regions. 1 month. Hipp: $t = 10.58$, d.f. = 8, ****$P < 0.0001$. Thal: $t = 14.092$, d.f. = 8, **$P = 0.0035$. Str: $t = 12.05$, d.f. = 8, ****$P < 0.0001$. PC: $t = 9.834$, d.f. = 8, ****$P < 0.0001$. MC: $t = 10.85$, d.f. = 8, ****$P < 0.0001$. HTT: $n = 5$, NTC: $n = 5$. 4 months. Hipp: $t = 6.117$, d.f. = 9, ***$P = 0.0002$. Thal: $t = 5.661$, d.f. = 9, ***$P = 0.0003$. Str: $t = 6.261$, d.f. = 9, ***$P = 0.0001$. PC: $t = 4.651$, d.f. = 9, **$P = 0.0012$, MC: $t = 3.46$, d.f. = 9, **$P = 0.0072$. HTT: $n = 6$, NTC: $n = 5$. 6 months. Hipp: $t = 19.01$, d.f. = 7, ****$P < 0.0001$. Thal: $t = 93.536$, d.f. = 7, **$P = 0.0095$. Str: $t = 3.479$, d.f. = 7, *$P = 0.0103$. HTT: $n = 5$, NTC: $n = 4$. **e**, di-siRNA *Htt* mRNA silencing shows a strong correlation with siRNA guide strand accumulation. **f**, di-siRNA HTT protein silencing shows a strong correlation with siRNA guide strand accumulation (IC_{50} ~ 0.5 μg g^{-1}). **g**, siRNA guide strand retention shows strong, two-phase tissue clearance kinetics. The majority of the compound is cleared within the first month. Clearance slows between 4 and 6 months. Mean ± s.d.

putamen (1 μg g^{-1}). We found cortical accumulation across seven slices spanning the entire brain (both ipsilateral and contralateral biopsies), confirming microscopy observations (Supplementary Fig. 16). In all NHP brain regions, guide strand accumulation level was well above the established IC_{50} value of ~0.5 μg g^{-1} (Fig. 2f).

To evaluate di-siRNA^{HTT} efficacy, we assessed *HTT* mRNA and protein expression in the NHP brain 1 month after injection. We observed potent silencing of mRNA expression in all brain regions, independent of the normalization control used (*PPIB* or *HPRT*) (Supplementary Fig. 17). There was no major difference in silencing between the ipsilateral and contralateral sides of the brain, which is consistent with uniform distribution. For protein silencing (Fig. 3f and Supplementary Fig. 18), we observed >90% silencing in the cortex ($P < 0.001$), >80% silencing in the hippocampus ($P < 0.01$), ~50–85% silencing in the caudate ($P < 0.001$) and ~40–70% silencing in the putamen ($P < 0.05$). These data indicate that a single

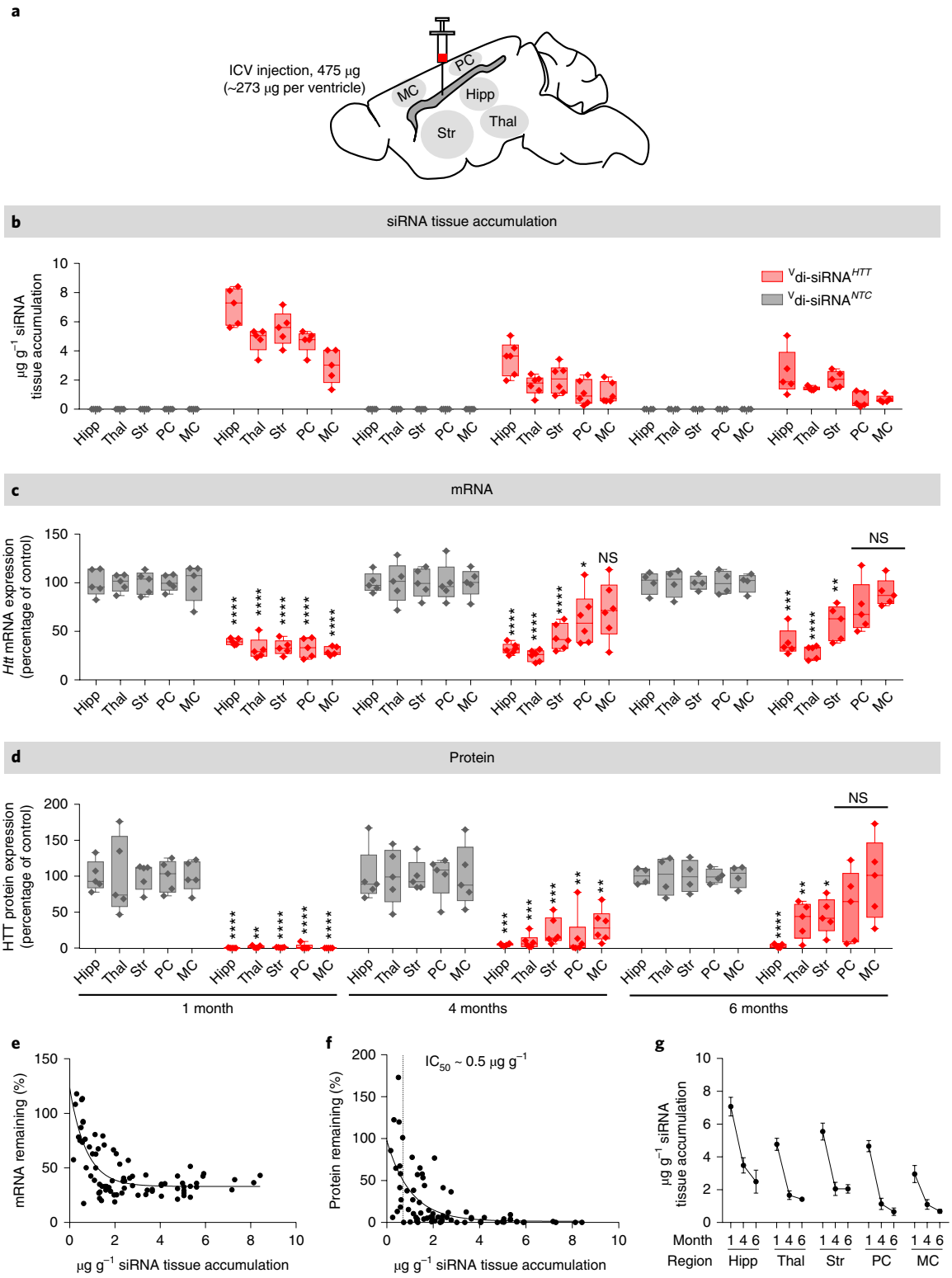

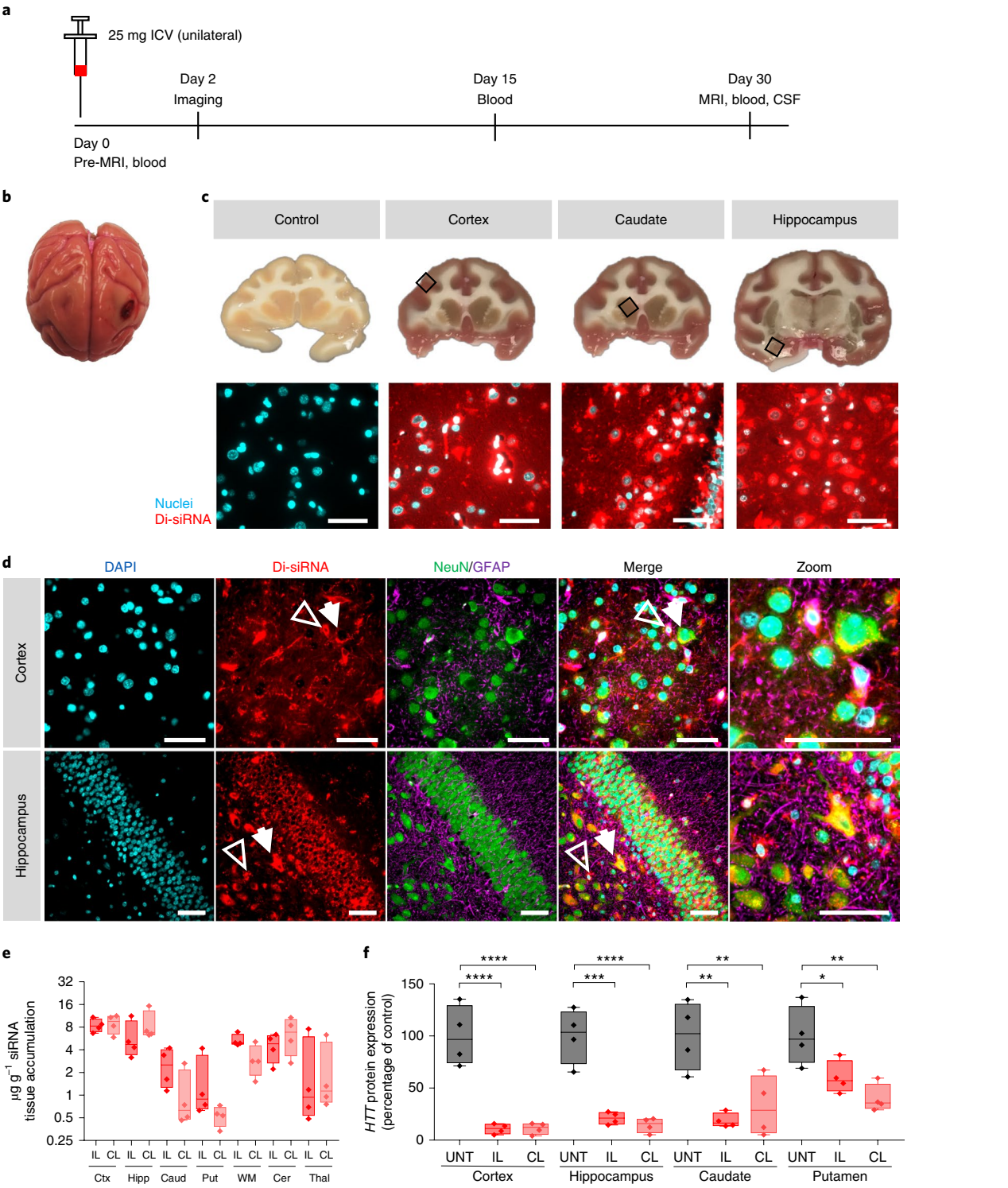

Fig. 3 | Gene silencing in the NHP CNS with di-siRNAs. Cynomolgus macaques received a unilateral ICV injection of di-siRNAs (25 mg). Samples were collected at 48 h for biodistribution and at 30 d for gene silencing and toxicity assessments. **a**, Schematic of NHP study. **b**, Image of whole NHP brain injected with Cy3-labeled di-siRNA. **c**, Images of NHP brain slices (top). Scale bar, 1 cm. High-resolution fluorescent images of di-siRNA in various regions of the NHP brain (bottom) Scale bar, 50 µm. **d**, Immunofluorescence of the NHP cortex and hippocampus. All images were acquired 48 h after a single unilateral ICV injection of 25 mg of di-siRNA. The hollow arrow indicates glial cells and the closed arrow indicates neurons. Scale bar, 50 µm. **e**, Quantification of siRNA guide strand ($n = 4$ treated animals, µg g^{-1}) in seven brain regions. IL, ipsilateral; CL, contralateral; Ctx, cortex; Hipp, hippocampus; Caud, caudate; Put, putamen; WM, white matter; Cer, cerebellum; Thal, thalamus. **f**, HTT protein silencing (percentage of control) IL and CL sides of four brain regions. UNT, untreated. Statistics were calculated by one-way ANOVA with Dunnet's correction for multiple comparisons. All results were compared to naive control. Cortex: $F(2,9) = 35.86$, $^{****}P < 0.0001$. Hippocampus: $F(2,9) = 35.15$, IL $^{***}P = 0.0001$, CL $^{****}P < 0.0001$. Caudate: $F(2,9) = 11.51$, IL $^{**}P = 0.0028$, CL $^{**}P = 0.0087$. Putamen: $F(2,9) = 9.08$, IL $^{*}P = 0.0385$, CL $^{**}P = 0.0043$. $n = 4$ per group. 1 month ($n = 4$ di-siRNA-treated animals, $n = 4$ naive animals). All graphs are mean ± s.d.

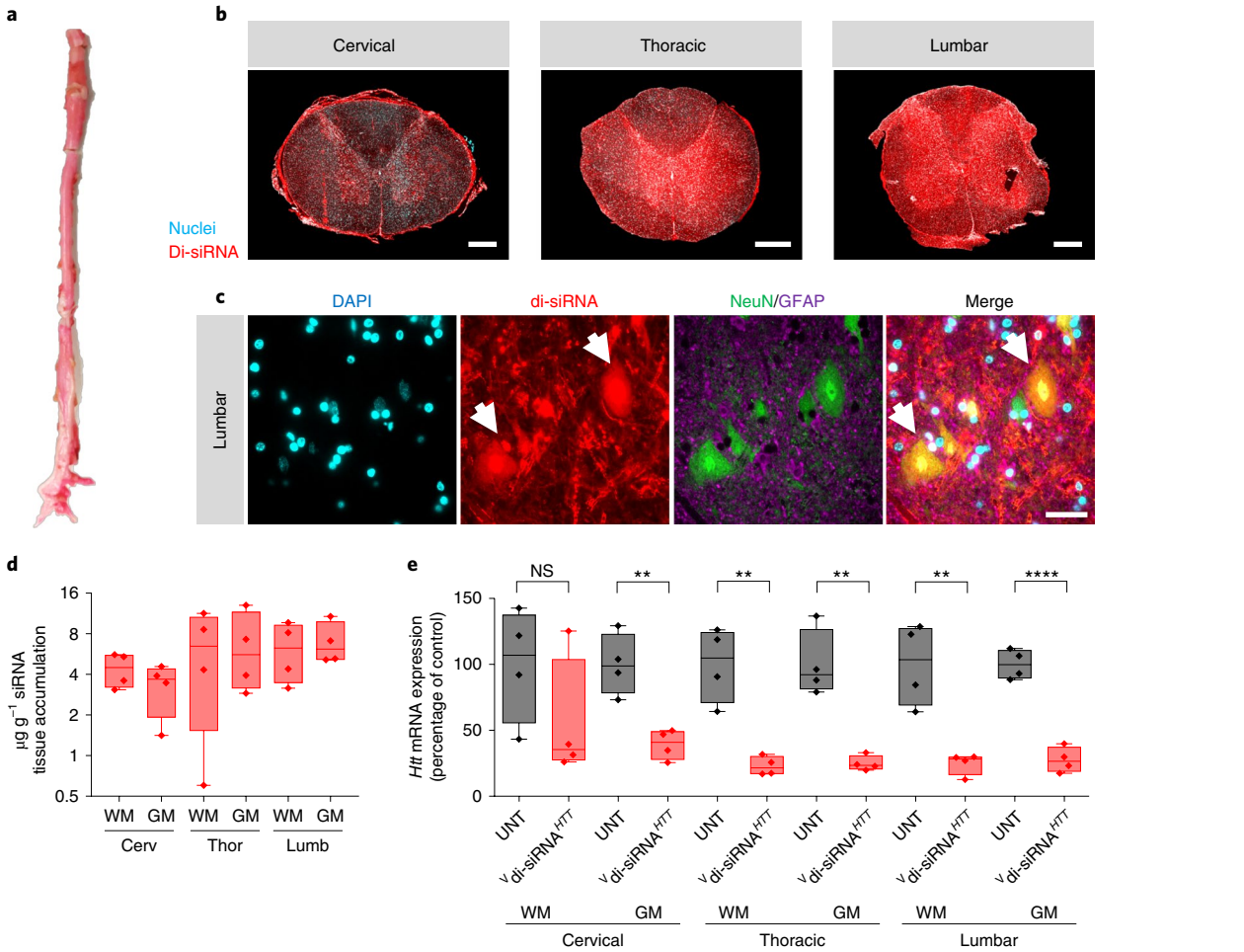

Fig. 4 | Di-siRNA enables silencing in the spinal cord of NHPs. a, Image of the whole NHP spinal cord. **b**, Tiled fluorescent images of cross sections of the spinal cord at each segment. Scale bar, 1 mm. **c**, Immunofluorescence of the NHP spinal cord (cervical, thoracic and lumbar regions). All images were acquired 48 h after a single unilateral ICV injection of 25 mg of di-siRNA. Scale bar, 50 µm. **d**, Quantification of siRNA guide strand (µg g^{-1}) in three spinal cord regions, both white matter (WM) and gray matter (GM). Cerv, cervical; thor, thoracic; lumb, lumbar. **e**, *HTT* mRNA silencing in various regions of the NHP spinal cord. Statistics calculated by two-tailed unpaired *t*-test: Cervical GM: $t=4.686$, d.f. = 6, $^{**}P=0.0034$. Thoracic WM: $t=5.278$, d.f. = 6, $^{**}P=0.0019$. Thoracic GM: $t=5.757$, d.f. = 6, $^{**}P=0.0012$. Lumbar WM: $t=4.69$, d.f. = 6, $^{**}P=0.0034$. Lumbar GM: $t=9.853$, d.f. = 6, $^{****}P<0.0001$. 1 month ($n=4$ di-siRNA-treated animals, $n=4$ naive animals). All graphs are mean ± s.d.

injection of di-siRNA enables silencing of target gene expression throughout the NHP brain.

Di-siRNA distributes and silences in the NHP spinal cord. The cortex and striatum are the two brain regions primarily affected in HD; however, treatment of other neurodegenerative disorders (for example, amyotrophic lateral sclerosis (ALS)) may require gene modulation in the spinal cord. We evaluated di-siRNA distribution and efficacy throughout the spinal cord 1 month after injection (Fig. 4). We observed robust distribution to all spinal cord regions, with guide strand accumulation ranging from 4–7 µg g^{-1} (Fig. 4d). Slightly higher accumulation was seen in the lumbar region compared to the cervical region. In all sections tested, we observed efficient delivery to all cell types, including neurons. Immunofluorescent images of the ventral horn of the lumbar spinal cord segment indicate robust delivery to lower motor neurons, easily identified morphologically by their large soma (Fig. 4c). Again, the level of guide strand accumulation was sufficient for potent *HTT* mRNA silencing in all regions tested ($P<0.01$), with the exception of a single outlier in cervical white matter (Fig. 4e).

Absence of detectable adverse events. We next looked at overall safety and tolerability of a single injection of 25 mg of di-siRNA in NHPs. MRI is commonly used to look at brain inflammation and edema. MRIs were collected preoperatively and 1 month following injection. There was no detectable difference between these scans, indicating that di-siRNA injection did not cause a major inflammatory response (Fig. 5a). Consistent with this finding, we did not observe substantial upregulation of *IBA-1* and *GFAP* at 1 month after injection (Fig. 5b,c). To determine whether there was any effect on neuronal viability, we examined two additional markers by western blot, NeuN[36] and BF-1 (ref. [37]). We observed no differences between naive and treated animals (Supplementary Fig. 19). In addition, we found no measurable changes in blood chemistry or cell counts (Supplementary Fig. 20), which is particularly important because thrombocytopenia (low platelet count) has been reported as a PS-mediated rare adverse event[13,14].

Finally, we sent treated and naive NHP brain sections for independent neuropathological analysis. No histopathological changes, with the exception of changes resulting directly from the needle track, were identified (Supplementary Note 2).

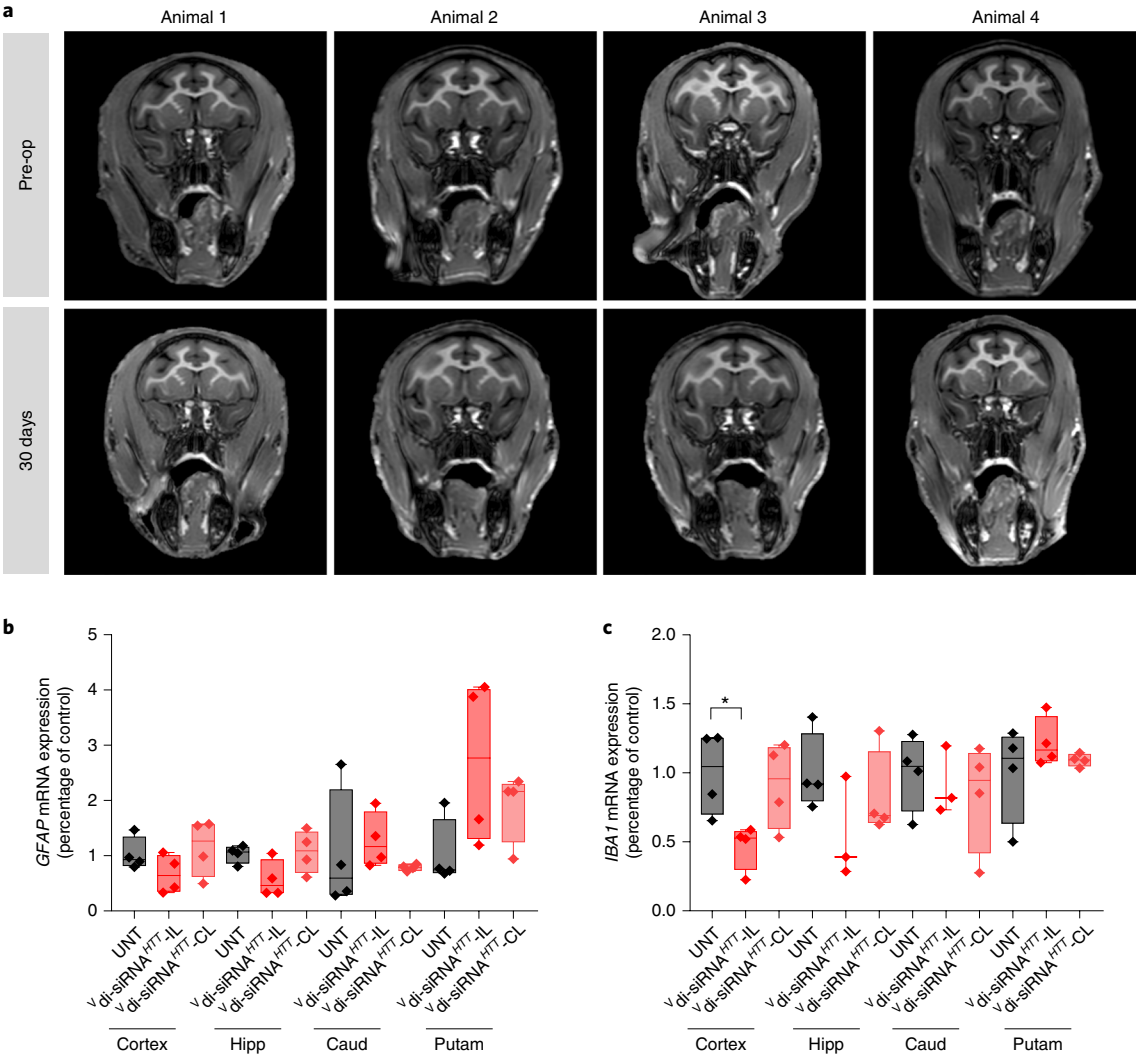

Fig. 5 | Assessment of brain toxicity 1 month after a single ICV injection of di-siRNA in NHPs. Animals were all dosed with 25 mg of di-siRNA unilaterally into the lateral ventricle. **a**, Preoperative and post-operative (30 d) MRI scans. **b**, *GFAP* mRNA expression was assessed 30 d after a single ICV injection. Hipp, hippocampus; Caud, caudate; Putam, putamen. **c**, *IBA-1* mRNA expression 30 d after a single ICV injection. Statistics calculated by one-way ANOVA with Dunnet's correction for multiple comparisons. All results were compared to naive controls. $F(2,9) = 4.578$ iplsilateral, $^*P < 0.0359$. $n = 4$ per group.

Di-siRNA modulates *HTT* expression with minimal off-target events. To determine whether *HTT* silencing or di-siRNA treatment had any major effect on the transcriptome, we performed genome-wide RNA sequencing (RNA-seq), comparing di-siRNA^{HTT}-treated to naive NHP brains. We analyzed three cortical replicates from each of eight animals (four naive, four treated). We chose to analyze the cortex, because we observed the highest accumulation of di-siRNA in this region and reasoned that the chances of seeing off-target effects would be highest here.

We observed 52 genes with significant differential expression between treated and naive animals, using a 1% false discovery rate (FDR) significance threshold (Fig. 6a and Supplementary Table 2). As expected, *HTT* was a single outlier with the most significantly impacted mRNA levels (75% silencing, $P < 10^{-40}$). Most other gene expression changes were minimal.

The siRNA off-target effects are a major concern in the development of siRNA-based therapeutics[38]. The siRNA off-target effects are predominantly due to seed (positions 2–7 of the guide strand) complementarity in the 3′ UTR of other targets[39]. To evaluate whether the observed non-*HTT* gene expression changes were due to the off-target effects of the siRNA, we looked at enrichment for seed complementarity in significantly downregulated and upregulated targets. Downregulated transcripts were slightly enriched for perfect complementarity to the guide strand seed region ($P = 0.04$), while no enrichment was observed in upregulated genes ($P = 0.59$). No enrichment was observed for seed reverse complement. The off-target effects observed in this study are minor in comparison to a previous study evaluating RNA-seq data in siRNA-treated rat liver[38].

To look more broadly at potential seed enrichment, we searched all differentially expressed 3′ UTRs for any combination of six nucleotides (seed length) that were overrepresented. For genes differentially expressed at a 1% FDR, there were no substantially overrepresented 6-mers and the HTT siRNA seed complement, AGAUUA, was present in the middle of the distribution (Fig. 6b). Relaxing the differential expression threshold to 10% FDR, there were several overrepresented 6-mers, but none of them matched AGAUUA (Supplementary Fig. 21).

There were seven differentially expressed genes whose 3′ UTRs contain the AGAUUA seed complement (Fig. 6c). For five out of seven transcripts, the changes were minor and are likely not biologically meaningful. There were only two potential genes, *APOLD1*

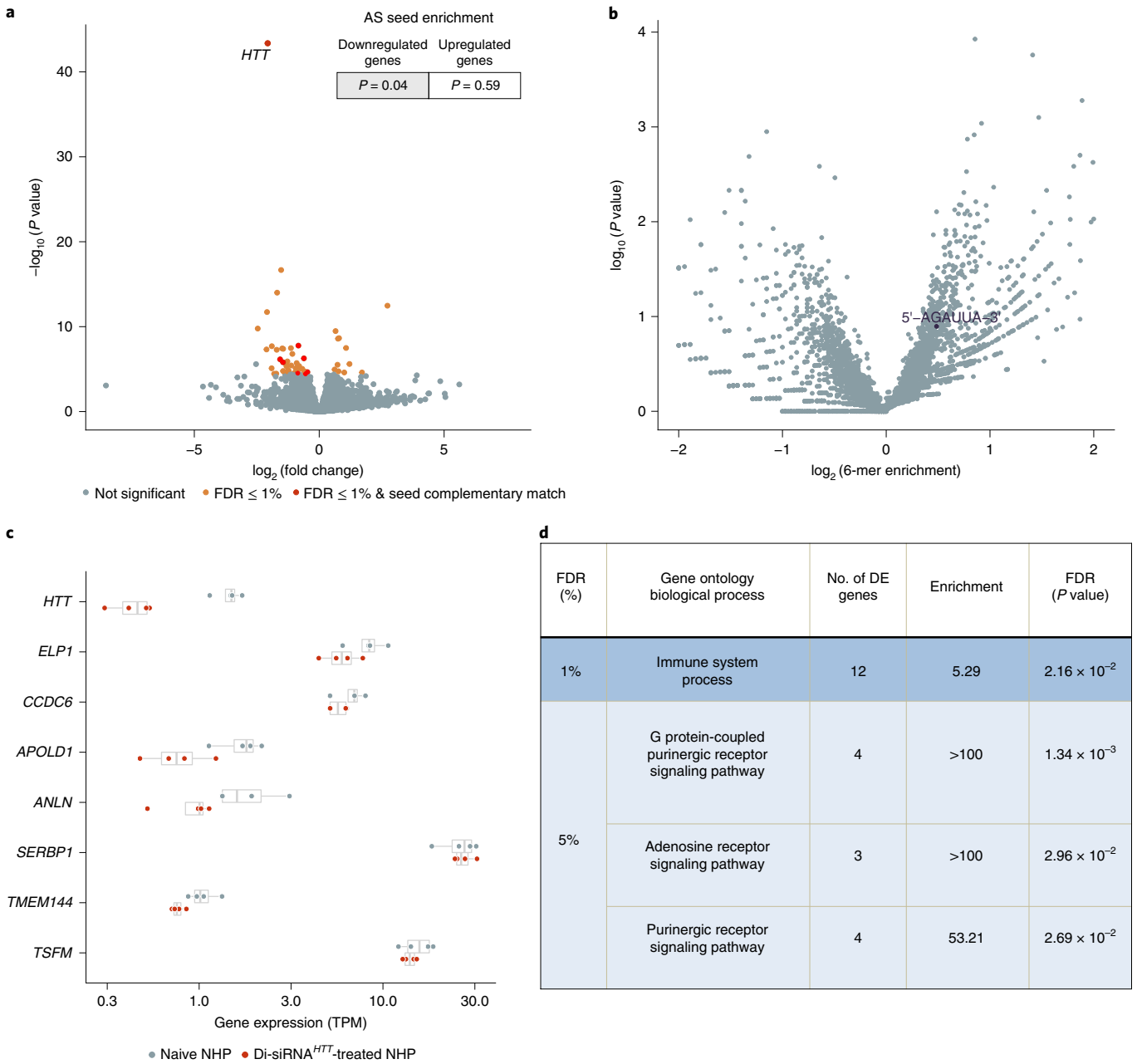

d

FDR (%)	Gene ontology biological process	No. of DE genes	Enrichment	FDR (*P* value)
1%	Immune system process	12	5.29	2.16×10^{-2}
5%	G protein-coupled purinergic receptor signaling pathway	4	>100	1.34×10^{-3}
	Adenosine receptor signaling pathway	3	>100	2.96×10^{-2}
	Purinergic receptor signaling pathway	4	53.21	2.69×10^{-2}

Fig. 6 | RNA-seq shows limited off-target effects of di-siRNA. RNA collected from cynomolgus macaques was subjected to RNA sequencing to assess genome-wide patterns of differential gene expression. **a**, Volcano plot showing genome-wide gene expression changes in di-siRNA^{HTT}-treated NHPs, with differentially expressed genes (Benjamini Hochberg FDR < 1%) in orange and differentially expressed genes with a 3′ UTR seed complementary region in red. Enrichment of 3′ UTR seed complementarity downregulated or upregulated genes (top right) was calculated using a Fisher's exact test. **b**, Volcano plot showing unbiased screen for enriched 6-mer sequences within 3′ UTRs of differentially expressed gene (FDR < 1%). There are no significantly over- or under-represented sequences after Benjamini Hochberg multiple test correction. Seed complementary sequence for di-siRNA^{HTT} is indicated in black. **c**, Gene expression measurements (transcripts per million, *x* axis) across four naive NHPs (gray) and four di-siRNA^{HTT}-treated NHPs (red) for the eight differentially expressed genes with seed complementary regions. **d**, Significant gene ontology categories for differentially expressed (DE) genes with FDR < 1% and FDR < 5%.

(~40% down) and *ANLN* (~20% down), that may be downregulated owing to miRNA-like off-target silencing.

HTT is involved in several cellular processes[40], raising the potential for transcriptional changes downstream of HTT silencing (on-target versus off-target effects). To determine whether changes were due to the on-target effects of HTT silencing, we performed gene ontology analyses on the differentially expressed genes. With a 1% FDR, only the 'immune system processes' category was enriched among differentially expressed genes, with 12 out of 576 expressed genes in this category showing differential expression.

With a 5% FDR, three other pathways were slightly enriched (Fig. 6d): G-protein-coupled purinergic receptors signaling, adenosine receptor signaling and purinergic receptor signaling. It is currently unknown whether the observed minor transcriptional changes are of biological relevance and, if so, whether they were caused by the trauma of ICV injection, HTT silencing, or

off-target silencing. In general, RNA-seq analyses of di-siRNA^{HTT}-treated NHP brains reveal no major transcriptional changes (aside from *HTT* silencing) and minimal, if any, off-targeting activity. Thus, di-siRNA enables highly specific silencing of gene expression in the CNS.

Discussion

Many technologies are being explored for gene modulation in the CNS, including adeno-associated virus (AAV) and ASOs[4,41,42]. AAV delivered by intraparenchymal injections efficiently silenced HTT in minipig, sheep and NHP[41,43,44]. However, multiple injections of AAV are required owing to the limited distribution achieved with a single injection. Major advances in AAV delivery are needed for uniform silencing throughout the brain. ASOs have enabled ~50% decrease of soluble mutant HTT in the CSF of patients following monthly intrathecal injections[45]. However, ASO delivery to deep brain structures is limited[4], without substantial HTT silencing observed in NHP caudates after multiple injections[42].

Here we have shown that divalent, PS-containing, fully chemically modified siRNAs achieve widespread distribution and silencing after a single bolus injection in rodent and NHP brains. Bulk flow of CSF is thought to be the primary mechanism driving broad oligonucleotide distribution and clearance in the brain. Thus, the difference in size between ASOs (7 kD) and di-siRNAs (27 kD) may contribute to the difference in distribution to deep brain structures. Linking of two ASOs via their 5′ ends resulted in better systemic efficacy compared to monomeric ASO variants[46].

di-siRNAs are comprised of two PS-containing siRNAs, with 26 PS modifications per molecule. Elimination of PS content completely abolished efficacy (Supplementary Fig. 4), suggesting that enhanced brain retention and distribution depends on PS modifications. The underlying mechanism is not fully understood, but multiple cell surface receptors have been recently identified that may be involved in phosphorothioate-mediated oligonucleotide uptake[15]. Our findings are consistent with recent efforts to fine-tune ASO potency and toxicity profiles via optimization of PS content (Moazami et al., personal communication). The level of PS modification in each strand of di-siRNAs (~40% phosphorothioated) is not sufficient to promote retention of monomers. Yet, by increasing the size and linking two siRNAs, the cooperativity of weak PS-driven cellular interactions produces robust cellular uptake and retention. Because increasing the percentage of PS modifications in the siRNA, either uniformly (that is, every other nucleotide linkage) or strategically, may interfere with RISC[17,18] and reduce tolerability, a multivalency approach may be preferable for fine-tuning siRNA uptake and toxicity.

We show that, in mice, duration of effect can be predicted based on compound tissue accumulation at earlier time points (1 month). In NHPs, we observed potent silencing in all brain regions at 1 month after injection. Given the level of accumulation in the cortex and hippocampus, silencing is expected to last 6–9 months in these regions, and as long as 2–4 months in the caudate and putamen. Therefore, repetitive injections would be necessary to maintain *HTT* silencing throughout the brain.

Animals with a single treatment of di-siRNA targeting *HTT* showed silencing of *HTT* with minimal transcriptome-wide changes. The miRNA-like off-target effects were observed for only two genes. Although seed complementary sequences were slightly overrepresented in the 3′ UTRs of downregulated transcripts, the overall effect and degree of enrichment was minimal compared to previously observed off-target effects with siRNA in rat livers[38] and in cells[47]. Off-target effects were explored in cortical samples, where guide strands accumulated to more than 9 μg g^{-1} and resulted in >90% HTT protein silencing. Substantially lower accumulation is sufficient for target silencing; therefore, the minimal off-target effects in this region are likely representative of transcriptome changes at high guide strand concentration. It is unclear whether the minimal level of off-target effects is specific to CNS regions, NHPs or these particular compounds because no other genome-wide off-targeting data in NHPs are available for comparison. However, our findings are consistent with published data in adult mice demonstrating that eliminating HTT causes minimal off-target phenotypes[48]. Although a lack of major transcriptional changes is consistent with the notion that there is no major perturbation of miRNA machinery, further investigations are required to detect changes in small RNA function.

It is currently unclear whether nonselective or single-nucleotide polymorphism-selective *HTT* silencing is a better therapeutic strategy for HD; however, a nonselective strategy would allow for treatment of all patients with HD with a single entity[49]. Di-siRNA is delivered to most cortical neurons, resulting in nonselective, potent silencing of wild-type and mutant HTT in the CNS, independent of brain size. Further evaluation in established disease models is necessary to assess the safety and efficacy of di-siRNA-mediated silencing of HTT and other targets.

Online content

Any methods, additional references, Nature Research reporting summaries, source data, statements of code and data availability and associated accession codes are available at https://doi.org/10.1038/s41587-019-0205-0.

Received: 25 October 2018; Accepted: 27 June 2019;
Published online: 2 August 2019

References

1. Khvorova, A. & Watts, J. K. The chemical evolution of oligonucleotide therapies of clinical utility. *Nat. Biotechnol.* **35**, 238–248 (2017).
2. Ostergaard, M. E. et al. Efficient synthesis and biological evaluation of 5'-galnac conjugated antisense oligonucleotides. *Bioconjug. Chem.* **26**, 1451–1455 (2015).
3. Rajeev, K. G. et al. Hepatocyte-specific delivery of siRNAs conjugated to novel non-nucleosidic trivalent N-acetylgalactosamine elicits robust gene silencing in vivo. *Chembiochem.* **16**, 903–908 (2015).
4. Kordasiewicz, H. B. et al. Sustained therapeutic reversal of Huntington's disease by transient repression of huntingtin synthesis. *Neuron.* **74**, 1031–1044 (2012).
5. Finkel, R. S. et al. Nusinersen versus sham control in infantile-onset spinal muscular atrophy. *N. Engl. J. Med.* **377**, 1723–1732 (2017).
6. Coelho, T. et al. Safety and efficacy of RNAi therapy for transthyretin amyloidosis. *N. Engl. J. Med.* **369**, 819–829 (2013).
7. Alterman, J. F. et al. Hydrophobically modified siRNAs silence huntingtin mRNA in primary neurons and mouse brain. *Mol. Ther. Nucleic Acids* **4**, e266 (2015).
8. Nikan, M. et al. Docosahexaenoic acid conjugation enhances distribution and safety of siRNA upon local administration in mouse brain. *Mol. Ther. Nucleic Acids* **5**, e344 (2016).
9. Osborn, M. F. & Khvorova, A. Improving small interfering RNA delivery in vivo through lipid conjugation. *Nucleic Acid Ther.* **28**, 128–136 (2018).
10. Nikan, M. et al. Synthesis and evaluation of parenchymal retention and efficacy of a metabolically stable O-Phosphocholine-N-docosahexaenoyl-l-serine siRNA conjugate in mouse brain. *Bioconjug. Chem.* **28**, 1758–1766 (2017).
11. Ly, S. et al. Visualization of self-delivering hydrophobically modified siRNA cellular internalization. *Nucleic Acids Res.* **45**, 15–25 (2017).
12. Eckstein, F. Phosphorothioates, essential components of therapeutic oligonucleotides. *Nucleic Acid Ther.* **24**, 374–387 (2014).
13. Flierl, U. et al. Phosphorothioate backbone modifications of nucleotide-based drugs are potent platelet activators. *J. Exp. Med.* **212**, 129–137 (2015).
14. Sewing, S. et al. Assessing single-stranded oligonucleotide drug-induced effects in vitro reveals key risk factors for thrombocytopenia. *PLoS ONE* **12**, e0187574 (2017).
15. Crooke, S. T., Wang, S., Vickers, T. A., Shen, W. & Liang, X. H. Cellular uptake and trafficking of antisense oligonucleotides. *Nat. Biotechnol.* **35**, 230–237 (2017).
16. Hassler, M. R. et al. Comparison of partially and fully chemically-modified siRNA in conjugate-mediated delivery in vivo. *Nucleic Acids Res.* **46**, 2185–2196 (2018).
17. Behlke, M. A. Progress towards in vivo use of siRNAs. *Mol. Ther.* **13**, 644–670 (2006).

18. Winkler, J., Stessl, M., Amartey, J. & Noe, C. R. Off-target effects related to the phosphorothioate modification of nucleic acids. *Chem. Med. Chem.* **5**, 1344–1352 (2010).
19. Amarzguioui, M., Holen, T., Babaie, E. & Prydz, H. Tolerance for mutations and chemical modifications in a siRNA. *Nucl. Acids Res.* **31**, 589–595 (2003).
20. Harborth, J. et al. Sequence, chemical, and structural variation of small interfering RNAs and short hairpin RNAs and the effect on mammalian gene silencing. *Antisense Nucl. Acid Drug Devel.* **13**, 83–105 (2003).
21. Nair, J. K. et al. Impact of enhanced metabolic stability on pharmacokinetics and pharmacodynamics of GalNAc-siRNA conjugates. *Nucleic Acids Res.* **45**, 10969–10977 (2017).
22. Fitzgerald, K. et al. A highly durable RNAi therapeutic inhibitor of PCSK9. *N. Engl. J. Med.* **376**, 41–51 (2017).
23. Ray, K. K. et al. Inclisiran in patients at high cardiovascular risk with elevated LDL cholesterol. *N. Engl. J. Med.* **376**, 1430–1440 (2017).
24. Lee, Y. C. et al. Binding of synthetic oligosaccharides to the hepatic Gal/GalNAc lectin. Dependence on fine structural features. *J. Biol. Chem.* **258**, 199–202 (1983).
25. Roehl, I., Schuster, M. & Seiffert, S. US Patent 20110201006 A1 (2011).
26. Liu, C. C., Liu, C. C., Kanekiyo, T., Xu, H. & Bu, G. Apolipoprotein E and Alzheimer disease: risk, mechanisms and therapy. *Nat. Rev. Neurol.* **9**, 106–118 (2013).
27. Mahley, R. W., Weisgraber, K. H. & Huang, Y. Apolipoprotein E4: a causative factor and therapeutic target in neuropathology, including Alzheimer's disease. *Proc. Natl Acad. Sci. USA* **103**, 5644–5651 (2006).
28. Zetterberg, H., Jacobsson, J., Rosengren, L., Blennow, K. & Andersen, P. M. Association of APOE with age at onset of sporadic amyotrophic lateral sclerosis. *J. Neurol. Sci.* **273**, 67–69 (2008).
29. Didiot, M. C. et al. Nuclear localization of huntingtin mRNA Is specific to cells of neuronal origin. *Cell. Rep.* **24**, 2553–2560 e2555 (2018).
30. Achuta, V. S. et al. Tissue plasminogen activator contributes to alterations of neuronal migration and activity-dependent responses in fragile X mice. *J. Neurosci.* **34**, 1916–1923 (2014).
31. Gu, X. et al. N17 Modifies mutant huntingtin nuclear pathogenesis and severity of disease in HD BAC transgenic mice. *Neuron* **85**, 726–741 (2015).
32. DiFiglia, M. et al. Huntingtin is a cytoplasmic protein associated with vesicles in human and rat brain neurons. *Neuron* **14**, 1075–1081 (1995).
33. Herndon, E. S. et al. Neuroanatomic profile of polyglutamine immunoreactivity in Huntington disease brains. *J. Neuropathol. Exp. Neurol.* **68**, 250–261 (2009).
34. Weyer, A. & Schilling, K. Developmental and cell type-specific expression of the neuronal marker NeuN in the murine cerebellum. *J. Neurosci. Res.* **73**, 400–409 (2003).
35. Takala, R. S. et al. Glial fibrillary acidic protein and ubiquitin C-Terminal hydrolase-L1 as outcome predictors in traumatic brain injury. *World Neurosurg.* **87**, 8–20 (2016).
36. Lind, D., Franken, S., Kappler, J., Jankowski, J. & Schilling, K. Characterization of the neuronal marker NeuN as a multiply phosphorylated antigen with discrete subcellular localization. *J. Neurosci. Res.* **79**, 295–302 (2005).
37. Dou, C. L., Li, S. & Lai, E. Dual role of brain factor-1 in regulating growth and patterning of the cerebral hemispheres. *Cereb. Cortex* **9**, 543–550 (1999).
38. Janas, M. M. et al. Selection of GalNAc-conjugated siRNAs with limited off-target-driven rat hepatotoxicity. *Nat. Commun.* **9**, 723 (2018).
39. Birmingham, A. et al. 3' UTR seed matches, but not overall identity, are associated with RNAi off-targets. *Nat. Methods* **3**, 199–204 (2006).
40. Zuccato, C., Valenza, M. & Cattaneo, E. Molecular mechanisms and potential therapeutical targets in Huntington's disease. *Physiol. Rev.* **90**, 905–981 (2010).
41. Evers, M. M. et al. AAV5-miHTT gene therapy demonstrates broad distribution and strong human mutant huntingtin lowering in a huntington's disease minipig model. *Mol. Ther.* **26**, 2163–2177 (2018).
42. Southwell, A. L. et al. Huntingtin suppression restores cognitive function in a mouse model of Huntington's disease. *Sci. Transl. Med.* **10**, eaar3959 (2018).
43. Pfister, E. L. et al. Artificial miRNAs reduce human mutant huntingtin throughout the striatum in a transgenic sheep model of Huntington's disease. *Hum. Gene. Ther.* **29**, 663–673 (2018).
44. Grondin, R. et al. Six-month partial suppression of huntingtin is well tolerated in the adult rhesus striatum. *Brain* **135**, 1197–1209 (2012).
45. Tabrizi, S. et al. Effects of IONIS-HTTRx in patients with early Huntington's disease, results of the first HTT-lowering drug trial (CT.002). *Neurology* **90**, CT.002 (2018).
46. Bhagat, L. et al. Novel oligonucleotides containing two 3'-ends complementary to target mRNA show optimal gene-silencing activity. *J. Med. Chem.* **54**, 3027–3036 (2011).
47. Malcolm, D. W., Sorrells, J. E., Van Twisk, D., Thakar, J. & Benoit, D. S. Evaluating side effects of nanoparticle-mediated siRNA delivery to mesenchymal stem cells using next generation sequencing and enrichment analysis. *Bioeng. Transl. Med.* **1**, 193–206 (2016).
48. Wang, G., Liu, X., Gaertig, M. A., Li, S. & Li, X. J. Ablation of huntingtin in adult neurons is nondeleterious but its depletion in young mice causes acute pancreatitis. *Proc. Natl Acad. Sci. USA* **113**, 3359–3364 (2016).
49. Pfister, E. L. et al. Five siRNAs targeting three SNPs may provide therapy for three-quarters of Huntington's disease patients. *Curr. Biol.* **19**, 774–778 (2009).

Acknowledgements

This project was funded by the NIH/NINDS (grant no. R01 NS104022; for A.K.), NIH/OD (grant no. S10 OD020012; for A.K.), CHDI (Research Agreement no. A-6119; for N.A.), Alzheimer's Drug Discovery Foundation (grant no. 20170101; for A.K.), Milton-Safenowitz Fellowship (no. 17-PDF-363; for B.M.D.C.G.) and The Berman–Topper Fund (for A.K. and N.A.). We would like to thank the University of Massachusetts Medical School Animal Medicine Department and veterinary technicians for their contributions to the large-animal studies. We would like to thank M.-C. Didiot for her mouse brain cartoon, E. Mohn and S. Hildebrand for editing the manuscript and Charles River Laboratories for help with neuropathology.

Author contributions

J.F.A., B.M.D.C.G., M.R.H. and A.K. conceived the project. J.F.A., B.M.D.C.G., M.R.H., C.M.F., M.D, N.A. and A.K. contributed to the experimental design. J.F.A., B.M.D.C.G., C.M.F, E.S., C.M.F., R.A.H., A.H.C., F.C., R.M., L.R., P.Y., A.A.T., E.G.K. and A.A.P. contributed experimentally. M.R.H. and D.E. synthesized the compounds. J.F.A., B.M.D.C.G., C.M.F., A.H.C., R.M.K., H.L.G.E., R.P.M., N.C.B., S.M.J., M.J.G. and M.S.E. carried out large-animal studies. G.G. and C.M. provided naive nonhuman primate samples. J.F.A., B.M.D.C.G., M.R.H., C.M.F. and A.K. wrote the manuscript.

Competing interests

A.K., J.F.A., M.R.H. and B.M.D.C.G. have filed a patent application for branched oligonucleotides.

Additional information

Supplementary information is available for this paper at https://doi.org/10.1038/s41587-019-0205-0.

Reprints and permissions information is available at www.nature.com/reprints.

Correspondence and requests for materials should be addressed to A.K.

Publisher's note: Springer Nature remains neutral with regard to jurisdictional claims in published maps and institutional affiliations.

Methods

Oligonucleotide synthesis, deprotection and purification. Oligonucleotides were synthesized using modified (2′-F, 2′-OMe) phosphoramidite with standard protecting groups. Solid-phase synthesis conditions using a MerMade 12 (BioAutomation) or AKTA Oligopilot 100 (GE Healthcare Life Sciences) using modified protocols. Unconjugated antisense oligonucleotide strands were grown on controlled pore glass functionalized with a long-chain alkyl amine and unylinker terminus (Chemgenes; no. N-4000-10). Sense strands, as divalent oligonucleotides were synthesized on modified solid support (Supplementary Fig. 1), made in-house to produce divalent sense strands. Phosphoramidites (ChemGenes) were prepared at 0.15 M (MerMade 12) and 0.2 M (AKTA) in acetonitrile (ACN) with added 15% dimethylformamide (DMF) in the 2'-OMe U amidite. 5-(Benzylthio)-1H-tetrazole (BTT) was used as the activator at 0.25 M. Detritylations were performed using 3% trichloroacetic acid in dichloromethane on the MerMade 12 and 3% dichloroacetic acid in toluene on the AKTA Oligopilot (AIC). Capping was done with non-tetrahydrofuran-containing reagents CAP A, 20% *n*-methylimidazole in ACN and CAP B, 20% acetic anhydride (Ac_2O), 30% 2,6-lutidine in ACN (AIC). Sulfurization was performed with 0.1 M solution of 3-[(dimethylaminomethylene)amino]-3H-1,2,4-dithiazole-5-thione (DDTT) in pyridine (ChemGenes) for 3 min. Phosphoramidite coupling times were 8 min for all amidites used.

Vinyl phosphonate deprotection. The vinylphosphonate containing oligo, while still on solid support, were treated post synthesis with a mixture of trimethylsilyl bromide/DMF/pyridine (1:9:0.5) for 1 h at room temperature with gentle agitation. The control pore glass was then rinsed with 10 ml of DMF followed by 10 ml of water, 10 ml of ACN and allowed to dry. Before being deprotected normally as described below.

Deprotection and purification of oligonucleotides. Both sense and antisense strands were cleaved and deprotected using 40% aq. methylamine at 45 °C for 60 min. The oligonucleotide solutions were then cooled in a freezer for a few minutes and filtered to remove the conrol pore glass from the cleaved oligo. The filtrate was then cooled with dry ice then dried under vacuum in a Speedvac. The resulting pellets were re-suspended in 5% ACN in water. The purification of antisense strands was performed on an Agilent 1100 series system, equipped with an Agilent PL-SAX, polymer ion exchange column (50 × 150 mm^2), or sourceQ anion exchange resin (GE Healthcare) (50 × 200 mm^2 custom-packed column) using the following conditions: eluent A, 20% ACN, 20 mM NaAc pH 8; eluent B, 1 M sodium perchlorate in 20% ACN; gradient, 0% B 2 min, 35% B 12 min, clean and re-equilibration to initial conditions at 50 ml min^{-1}. Purification of sense strands was performed on the same equipment but equipped with a PRP-C18, a polymer reverse phase column (4.6 × 150 mm^2), using the following conditions: eluent A, 50 mM sodium acetate in 5% ACN; eluent B, ACN; gradient, 0% B 2 min, 0–40% B 1 min, 40–70% B 8 min, clean and re-equilibration 6 min. Temperature, 70 °C, and flow rate, 50 ml min^{-1}, were the same in both cases. Peaks were monitored at 280 nm. The pure oligonucleotides fractions were collected, individually characterized by liquid chromatography–mass spectromery (LC–MS), combined, frozen and dried in a Speedvac overnight. Oligonucleotides were re-suspended in 5% ACN, and desalted through fine Sephadex G-25 columns (50 × 300 mm^2), and lyophilized. All reagents mentioned above were purchased from Sigma Aldrich and used as per manufacturer's instructions, unless otherwise stated.

LC–MS analysis of oligonucleotides. The identity of oligonucleotides were established by LC–MS analysis on an Agilent 6530 accurate mass Q-TOF LC–MS machine using the following conditions: buffer A: 100 mM hexafluoroisopropanol/9 mM triethylamine in LC–MS grade water; buffer B:100 mM hexafluoroisopropanol/9 mM triethylamine in LC–MS grade methanol; column, Agilent AdvanceBio oligonucleotides C18; gradient antisense, 0% B 1 min, 0–30% B 8 min, clean and re-equilibration 4 min; gradient sense, 0% B 1 min, 0–50% B 0.5 min, 50–100% B 8 min, clean and re-equilibration 4 min; temperature, 45 °C; flow rate, 0.5 ml min^{-1}, UV (260 nm). MS parameters: source, electrospray ionization; ion polarity, negative mode; range, 100–3,200 *m*/*z*; scan rate, 2 spectra s^{-1}; capillary voltage, 4,000; fragmentor, 180 V. All reagents mentioned above were purchased form Sigma Aldrich and used as per manufacturer's instructions, unless otherwise stated.

Cell culture and in vitro screening. As described previously by Hassler et al.[16], briefly, HeLa cells were treated with RNAiMax (13778-150) formulated Mono-siRNAs and di-siRNAs for 72 h in 50:50 DMEM (Cellgro, 10-013-CV)/OptiMEM (Gibco, 31985-070) with 3% FBS and no PS. Cells were then lysed in diluted lysis mixture, 1 part lysis mixture (Invitrogen, 13228) and 2 parts water with proteinase K (Invitrogen, 25530-049). mRNA was detected according to the Quantigene 2.0 protocol using the following probe sets: human HTT (SA-50339), human HPRT (SA-10030).

Animal studies. All experimental studies involving animals were approved by the University of Massachusetts Medical School Institutional Animal Care and Use Committee (IACUC Protocol nos. A-2411 and A-2515) and performed according to the guidelines and regulations therein described.

Stereotactic injections in rodents. FVB/NJ females (8–9 weeks old) or BACHD-ΔN17 females (6 weeks old) were anesthetized using 1.2% Avertin. Animals were kept under anesthesia for 2 hours after injection. Single intrastriatal administrations (2 µl per injected side) were performed as previously described[8,10] at the following coordinates from bregma: +1.0 mm anterior-posterior (AP) ±2.0 mm mediolateral and −3.0 mm dorsoventral. Single bilateral intracerebroventricular injections (5 µl per injected side) were performed at 500 nl min^{-1} after needle placement at the following coordinates from bregma: −0.2 mm AP, ±0.8 mm mediolateral and −2.5 mm dorsoventral. Doses of mono-siRNA and di-siRNA ranged between 4 nmol (50 µg) and 40 nmol (475 µg) according to the goal of the experiment.

For biodistribution studies, animals ($n = 2–3$ per group) were euthanized at 48 h after injection and perfused with PBS. Brains were harvested and post-fixed overnight with 10% formalin and processed for paraffin embedding. For efficacy studies, animals ($n = 6–8$ per group) were euthanized at different time points, including 1, 2 weeks and 1, 3, 4, 6 months after single intracranial injections. At harvesting, tissues were kept in RNA later overnight (mRNA analysis) and then stored in −80 °C, or snap frozen (western blot assessments) and stored.

Stereotactic injection in NHPs. Cynomolgus macaques (2.5–4.5 kg) were sedated using ketamine (15 mg kg^{-1}), xylazine (0.5 mg kg^{-1}) and glycopyrolate (0.01 mg kg^{-1}), and a tracheal tube placed. Anesthesia was maintained by isoflurane 1–3% carried by oxygen (1 l min^{-1}). Animals received intravenous lactate ringer solution at a rate of 5–10 ml kg h^{-1} and were placed on a heating blanket. Meloxicam (0.15 mg kg^{-1}) and buprenorphine (0.01 mg kg^{-1}) were given for analgesia. Respiratory rate, end tidal CO_2, body temperature, spO_2 and heart rate were monitored and recorded.

Standard surgical aseptic technique was used throughout the procedure. Macaques were positioned on a stereotaxic frame for NHPs (KOPF Model 1530 M) and the skin cleaned with alternating applications of betadine and alcohol. The skull was exposed by a transverse incision and the periosteum removed from the surgical area. Based on the positioning of bregma, a burr hole (3–5 mm) was drilled using a Stryker high-speed drill (core powered instrument driver and precision neuro drill bit (catalog no. 5820-107-530)). Real-time cone beam CT images were registered on preoperative MRI datasets (see details on MRI acquisition below) for determination of correct positioning of the manipulator for cannula placement. A cannula was lowered onto the left lateral ventricle and 50 µl of iodohexal contrast agent was administered followed by high-resolution cone beam CT to confirm correct positioning of the device. The US Food and Drug Administration-approved SmartFlow neuroventricular cannulas (16 ga, 0.2 mm internal diameter × 1.22 m, MRI Interventions, Inc.) were used for all ICV injections. Cannulas were attached to a syringe fitted in a programmable PhD Ultrapump (Harvard Apparatus).

Di-siRNAs (25 mg per 750 µl) were injected at a rate of 50 µl min^{-1} for 15 min, and anesthesia switched to propofol (1 ml h^{-1}). Cannulas were withdrawn 5–10 min after the end of the injections. The skull was irrigated with ~50 ml of 0.9% saline and scalp sutured with absorbable sutures (3-0 or 4-0 Vicryl Rapide) in an interrupted pattern. Animals were kept under anesthesia for ~2 h following the end of the ICV injection and were given prophylactic antibiotics (cephazolin, IV). Macaques were returned to their home cage to recover and monitored for signs of pain and distress.

Complete blood counts and a comprehensive blood chemistry panel was carried out on preoperative blood and after 2 d (distribution study), or 15 d and 30 d after injection (efficacy studies). For siRNA guide strand quantification, blood samples were collected preoperatively and at the following time points after di-siRNA injection: 5, 15, 30 min, 1 and 2 h.

At necropsy, animals were heparinized and euthanized with an intravenous injection of pentobarbital (150 mg kg^{-1}). CSF samples were immediately collected from the cisterna magna after euthanasia. Animals were then perfused with 4 l of sterile cold PBS, and tissues collected for mRNA, protein and histology.

Brain MRI. Preoperative and 30-d MRI scans were acquired using a Philips Achieva 3Tesla Whole Body Scanner. Animals were anesthetized as previously described and placed on a MRI-compatible stereotaxic frame in ventral recumbency (head first into the magnet). Axial T1 unenhanced spin-echo, axial T2 fast spin-echo, diffusion weighted imaging, magnetic resonance angiography and magnetization prepared rapid gradient echo sequences. In-plane resolution was 0.4 to 1 mm, slice thickness 1–4 mm and acquisition matrix 256 × 256. Total MRI time was approximately 60–90 min per subject. Following imaging, the animal was recovered from anesthesia and monitored in the cage.

mRNA quantification. Mouse brain tissue was harvested and placed in ice-cold PBS (Fisher, BP2438). Brains were sliced into 300 µm sections on a vibratome. The 2 mm punches were taken from each section. Punches from the left side were put into RNAlater (Sigma, R0901) for mRNA quantification.

NHP brains were perfused with ice-cold PBS (Fisher, BP2438) before sectioning. Brains were sectioned in a brain matrix into 4 mm sections. The 2 mm

punches were taken from various brain regions and placed in RNAlater (Sigma, R0901) for mRNA quantification.

As described previously[16], tissues were lysed in Quantigene 2.0 homogenizing buffer (Invitrogen, QG0517) with proteinase K (Invitrogen, 25530-049). mRNA was detected according to the Quantigene 2.0 protocol using the following probe sets: mouse HTT (SB-14150), mouse GFAP (SB-14051), mouse IBA-1 (SB-3027744), mouse HPRT (SB-15463), mouse PPIB (SB-10002), mouse APOE (SB-13611), NHP HTT (SF-10209), NHP GFAP (SF-4228397), NHP IBA-1 (SF-4214274) and NHP HPRT (SF-10356).

Protein quantification. Mouse tissue collection was performed as described above in the mouse mRNA tissue collection. Punches from the right side of brain were flash-frozen for western blot preparation.

NHP tissue collection was performed as follows: NHP brains were perfused with PBS before sectioning. Brains were sectioned in a brain matrix into 4 mm sections. The 2 mm punches were taken from various brain regions flash-frozen for western protein quantification.

Tissue processing was performed as described previously[7].

For analysis of APOE protein expression in mouse brain samples, WES by ProteinSimple was used. Tissue punches were collected as above and flash-frozen and placed at −80 °C. After addition of RIPA buffer with protease inhibitors, samples were homogenized and stored at −80 °C. Protein amount was determined using a Bradford Assay. Samples were diluted in 0.1× sample buffer (ProteinSimple) to ~0.2–0.4 μg μl^{-1}. Anti-APOE antibody (Abcam, 183597) was diluted 1:200 in antibody diluent (ProteinSimple) and loading control, anti-vinculin (Invitrogen, 700062), was diluted 1:600 in antibody diluent. Assay was performed as described by the ProteinSimple protocol using the 16–230 kDa plate (SM-W004).

Guide strand quantification. Conducted as described previously[16]. Briefly, guide strand was quantified by hybridization to a complementary peptide nucleic acid strand labeled with a Cy3 fluorescent dye. Accumulation was then measured by HPLC fluorescence detection and peak quantification.

Fluorescent imaging. Conducted as described previously[16]. Briefly, tissues for imaging were fixed overnight in (mouse) or for 7 d (NHP) in 10% neutral buffered formalin (Sigma, HT501320), and then transferred to PBS. All tissues were paraffin-embedded and sliced into 4 μm sections. Sections were stained with DAPI and imaged on a Leica inverted microscope. Staining for colocalization of di-siRNA with neuronal (NueN) and glial cells (GFAP) was performed as described previously[50].

RNA-seq. Total RNA was isolated from three brain punches each from eight animals, four naive and four di-siRNA^{HTT}-treated, using a Monarch Total RNA Miniprep Kit (NEB, T2010S) following the manufacturer's protocol. Briefly, tissue was submerged in DNA/RNA protection reagent, homogenized by passing through a 27 G hypodermic needle, and incubated for 30 min at −80 °C with proteinase K. RNA was bound to column, subjected to on-column DNase treatment, washed and eluted in nuclease-free water. Library preparation was performed using TruSeq Stranded mRNA Library Prep (Illumina, 20020594) following the manufacturer's protocol. Single-end sequencing was performed for 75 cycles on the Illumina NextSeq 500, for a total of 271.6 million reads (average of 33.9 million reads per animal).

The resulting 75-neucleotide reads were mapped to the cynomolgus macaque genome (*Macaca fascicularis* 5.0) with STAR v.2.5.3a. Reads mapping to annotated exons were counted using HTseq v.0.10.0 and differential expression analysis was performed with DESeq2 v.1.22.2. Genes that had fewer than 10 reads across all samples or were only expressed in one animal were excluded from further analyses. Seed complementary matches and enriched 6-mers within 3′ UTRs (for genes with annotated 3′ UTRs in *Macaca fascicularis* Ensembl 95 annotations) were identified using a custom python script. Gene set enrichment analysis was conducted using PANTHER v.14.0, conditioning on biological process gene ontology categories.

Statistics. All statistics were calculated using GraphPad Prism v.7. Box plots: center line, median; top of box, 75% quartile; bottom of box, 25% quartile; whiskers, minimum and maximum. Additional information can be found in the Reporting Summary.

Reporting Summary. Further information on research design is available in the Nature Research Reporting Summary linked to this article.

Data availability

The RNA-seq data from nonhuman primate samples have been deposited in GEO under accession code GSE130132, including processed transcriptome read counts.

References

50. Godinho, B. et al. Transvascular delivery of hydrophobically modified siRNAs: Gene silencing in the rat brain upon disruption of the blood-brain barrier. *Mol. Ther.* **26**, 2580–2591 (2018).

nature research

Corresponding author(s): Anastasia Khvorova

Last updated by author(s): 6/13/2019

Reporting Summary

Nature Research wishes to improve the reproducibility of the work that we publish. This form provides structure for consistency and transparency in reporting. For further information on Nature Research policies, see Authors & Referees and the Editorial Policy Checklist.

Statistics

For all statistical analyses, confirm that the following items are present in the figure legend, table legend, main text, or Methods section.

n/a	Confirmed	
☐	☒	The exact sample size (*n*) for each experimental group/condition, given as a discrete number and unit of measurement
☐	☒	A statement on whether measurements were taken from distinct samples or whether the same sample was measured repeatedly
☐	☒	The statistical test(s) used AND whether they are one- or two-sided *Only common tests should be described solely by name; describe more complex techniques in the Methods section.*
☒	☐	A description of all covariates tested
☐	☒	A description of any assumptions or corrections, such as tests of normality and adjustment for multiple comparisons
☒	☐	A full description of the statistical parameters including central tendency (e.g. means) or other basic estimates (e.g. regression coefficient) AND variation (e.g. standard deviation) or associated estimates of uncertainty (e.g. confidence intervals)
☐	☒	For null hypothesis testing, the test statistic (e.g. *F*, *t*, *r*) with confidence intervals, effect sizes, degrees of freedom and *P* value noted *Give P values as exact values whenever suitable.*
☒	☐	For Bayesian analysis, information on the choice of priors and Markov chain Monte Carlo settings
☒	☐	For hierarchical and complex designs, identification of the appropriate level for tests and full reporting of outcomes
☒	☐	Estimates of effect sizes (e.g. Cohen's *d*, Pearson's *r*), indicating how they were calculated

Our web collection on statistics for biologists contains articles on many of the points above.

Software and code

Policy information about availability of computer code

Data collection	N/A
Data analysis	Graphpad Prism, Microsoft Excel

For manuscripts utilizing custom algorithms or software that are central to the research but not yet described in published literature, software must be made available to editors/reviewers. We strongly encourage code deposition in a community repository (e.g. GitHub). See the Nature Research guidelines for submitting code & software for further information.

Data

Policy information about availability of data

All manuscripts must include a data availability statement. This statement should provide the following information, where applicable:

- Accession codes, unique identifiers, or web links for publicly available datasets
- A list of figures that have associated raw data
- A description of any restrictions on data availability

Data available

Field-specific reporting

Please select the one below that is the best fit for your research. If you are not sure, read the appropriate sections before making your selection.

☒ Life sciences ☐ Behavioural & social sciences ☐ Ecological, evolutionary & environmental sciences

For a reference copy of the document with all sections, see nature.com/documents/nr-reporting-summary-flat.pdf

Life sciences study design

All studies must disclose on these points even when the disclosure is negative.

Sample size	Sample size was calculated in IACUC protocol referenced in methods section.
Data exclusions	No exclusions
Replication	N/A
Randomization	Not randomized
Blinding	Not blinded

Reporting for specific materials, systems and methods

We require information from authors about some types of materials, experimental systems and methods used in many studies. Here, indicate whether each material, system or method listed is relevant to your study. If you are not sure if a list item applies to your research, read the appropriate section before selecting a response.

Materials & experimental systems

n/a	Involved in the study
☐	☒ Antibodies
☐	☒ Eukaryotic cell lines
☒	☐ Palaeontology
☐	☒ Animals and other organisms
☒	☐ Human research participants
☒	☐ Clinical data

Methods

n/a	Involved in the study
☒	☐ ChIP-seq
☒	☐ Flow cytometry
☐	☒ MRI-based neuroimaging

Antibodies

Antibodies used	Anti-ApoE antibody (Abcam, 183597). anti-Vinculin (Invitrogen, 700062). anti-NeuN Millipore, Taunton, MA; MAB377,. N-terminal antihuntingtin antibody Ab158. anti-β tubulin antibody (Sigma; #T8328). IBA-1 (Wako; #019-19741), Anti-Darpp32 (Abcam; #40801), 5TF1-1C2 (Millipore MAB1574)
Validation	antibodies were validated for each application using manufacturers guidelines. Multiple dilutions were tested to determine the most appropriate dilution.

Eukaryotic cell lines

Policy information about cell lines

Cell line source(s)	HeLa; ATCC.
Authentication	Authenticated
Mycoplasma contamination	Negative for contamination
Commonly misidentified lines (See ICLAC register)	*Name any commonly misidentified cell lines used in the study and provide a rationale for their use.*

Animals and other organisms

Policy information about studies involving animals; ARRIVE guidelines recommended for reporting animal research

Laboratory animals	Rodents: FVB/NJ, female NHP: Cynamolgos macaques, males and females
Wild animals	*Provide details on animals observed in or captured in the field; report species, sex and age where possible. Describe how animals were caught and transported and what happened to captive animals after the study (if killed, explain why and describe method; if released, say where and when) OR state that the study did not involve wild animals.*
Field-collected samples	*For laboratory work with field-collected samples, describe all relevant parameters such as housing, maintenance, temperature, photoperiod and end-of-experiment protocol OR state that the study did not involve samples collected from the field.*

Ethics oversight | *Identify the organization(s) that approved or provided guidance on the study protocol, OR state that no ethical approval or guidance was required and explain why not.*

Note that full information on the approval of the study protocol must also be provided in the manuscript.

Magnetic resonance imaging

Experimental design

Design type	N/A (no fMRI was used)
Design specifications	N/A (no fMRI was used)
Behavioral performance measures	N/A (no fMRI was used)

Acquisition

Imaging type(s)	Structural, DTI
Field strength	3.0T
Sequence & imaging parameters	MP-RAGE (T1-TFE): TR/TE: 11/5ms FA: 8, matrix 288x288, thickness 0.7mm, axial isotropic, FoV 120mm, ETL 153 T2W-TSE: TR/TE 7000/80ms, FA 90, matrix 432x432, thickness 1mm, axial, FoV 80x100mm ETL 22
Area of acquisition	whole brain scan

Diffusion MRI ☒ Used ☐ Not used

Parameters: 32 directions, b value 1000, single shell, no gating

Preprocessing

Preprocessing software	N/A
Normalization	N/A
Normalization template	N/A
Noise and artifact removal	N/A
Volume censoring	N/A

Statistical modeling & inference

Model type and settings	*Specify type (mass univariate, multivariate, RSA, predictive, etc.) and describe essential details of the model at the first and second levels (e.g. fixed, random or mixed effects; drift or auto-correlation).*
Effect(s) tested	*Define precise effect in terms of the task or stimulus conditions instead of psychological concepts and indicate whether ANOVA or factorial designs were used.*

Specify type of analysis: ☐ Whole brain ☐ ROI-based ☐ Both

Statistic type for inference (See Eklund et al. 2016)	*Specify voxel-wise or cluster-wise and report all relevant parameters for cluster-wise methods.*
Correction	*Describe the type of correction and how it is obtained for multiple comparisons (e.g. FWE, FDR, permutation or Monte Carlo).*

Models & analysis

n/a	Involved in the study
☒	☐ Functional and/or effective connectivity
☒	☐ Graph analysis
☒	☐ Multivariate modeling or predictive analysis